SCIENTIFIC REPORTS

OPEN

SUBJECT AREAS:
CELL BIOLOGY
PROTEOMICS
EPIGENETICS
STRUCTURAL BIOLOGY

Received
25 September 2012

Accepted
6 November 2012

Published
13 February 2013

Correspondence and requests for materials should be addressed to A.G.M. (marshall@magnet.fsu.edu) or J.C. (okachen30@gmail.com)

* These authors contributed equally to this work.

Nucleotide-induced conformational changes of tetradecameric GroEL mapped by H/D exchange monitored by FT-ICR mass spectrometry

Qian Zhang[1]*, Jin Chen[2]*, Kunihiro Kuwajima[2,3], Hui-Min Zhang[4], Feng Xian[4], Nicolas L. Young[4] & Alan G. Marshall[1,4]

[1]Florida State University, Department of Chemistry, Tallahassee, FL 32306, USA, [2]Okazaki Institute for Integrative Bioscience and Institute for Molecular Science, National Institutes of Natural Sciences, 5-1 Higashiyama, Myodaiji, Okazaki 444-8787, Japan, [3]Department of Functional Molecular Science, School of Physical Sciences, Graduate University for Advanced Studies (Sokendai), 5-1 Higashiyama, Myodaiji, Okazaki 444-8787, Japan, [4]National High Magnetic Field Laboratory, 1800 East Paul Dirac Drive, Tallahassee, FL 32310, USA.

Here we employ hydrogen/deuterium exchange mass spectrometry (HDX-MS) to access *E. coli* chaperonin GroEL conformation. The ~800 kDa tetradecameric GroEL plays an essential role in the proper folding of many proteins. Previous studies of the structural dynamics of GroEL upon ATP binding have been inconsistent, showing either minimal or major allosteric changes. Our results, based on the native, non-mutated, protein under physiological conditions in solution demonstrate substantial changes in conformation and/or flexibility upon ATP binding. We capture the pivotal step in its functional cycle by use of a non-hydrolyzable ATP analog, ATPγS, to mimic the ATP-bound GroEL state. Comparison of HDX-MS results for apo GroEL and GroEL-ATPγS enables the characterization of the nucleotide-regulated conformational changes throughout the entire protein with high sequence resolution. The 14-mer GroEL complex is the largest protein assembly yet accessed by HDX-MS, with sequence resolution of segments of as few as five amino acids.

In response to environmental stress, a cell employs molecular chaperones to maintain protein folding homeostasis. The most remarkable molecular chaperone in *E. coli*, chaperonin GroEL, aided by GroES, plays an essential role in the protein quality-control system[1–5]. More than 200 cytosolic proteins are known to interact with GroEL. Thus, the GroEL/GroES system has been intensively studied in attempts to understand the underlying mechanism of its mediated-folding of diverse substrate proteins[6–12,13].

GroEL is composed of 14 identical subunits of 57 kDa each (~800 kDa total), arranged in two homoheptameric rings stacked 'back to back' to form a cylinder with a central folding channel for substrate proteins. Each GroEL subunit consists of three functional domains: equatorial, intermediate, and apical. From the x-ray crystal structure of bacterial apo GroEL[1], the equatorial domain, which includes the ATP-binding site, serves as the foundation of the complex, providing most of the lateral intra-ring and inter-ring interactions between subunits. The intermediate domain, which is flanked by the apical and equatorial domains, serves as part of the outer surface of the cylinder wall. The apical domain forms the opening of the central channel.

To function *in vivo*, the GroEL complex undergoes coupled structural movements across its three subdomains, triggered by ATP binding to the equatorial domain[4,14–17]. It was recently found that ATP-binding to GroEL precedes the binding of the substrate protein and GroES[7,11]. Thus, structural characterization of the nucleotide-bound intermediate state and the associated conformational changes that occur before the binding of substrate protein are crucially important for understanding the overall chaperone cycle. Despite a host of studies aimed at dissecting the underlying mechanism of GroEL/GroES-mediated refolding of substrate proteins[7,9,10,18], the molecular details of GroEL during its functional cycle are sparse.

To capture the ATP regulated GroEL structure, previous attempts have employed X-ray crystallography, cryo-EM, and fluorescence spectroscopy. For X-ray crystallography, Boisvert et al. crystallized an ATPase activity-deficient double mutant GroEL complexed with ATPγS, with little structural difference compared to apo

GroEL[19]. Wang et al. crystallized a triple-mutant GroEL with ATPγS and then replaced ATPγS by ATP, but the ATP triggered an observable structure change only in the apical domain[20]. The X-ray crystallography data is in contradiction with the cryo-EM findings by Ranson et al., who observed ATP induced allosteric changes throughout the entire GroEL molecule. Such a paradox suggests that the solution structure of GroEL is not well characterized by X-ray crystallography. Based on fluorescence spectroscopy, Inobe et al.[21] observed no significant GroEL conformational changes triggered by ATPγS or AMP-PNP, perhaps due to incomplete sequence coverage (i.e., one or a few tryptophan probes for the entire GroEL molecule) and/or the sensitivity of fluorescence detection. Moreover, all of the above experiments were performed with GroEL mutants, which may not represent the true wild type GroEL.

HDX-MS offers a non-perturbative means to characterize protein higher-order structure and solvent accessibility[22–25] and protein-ligand/protein interactions[26–30]. Recently, several technical advances have improved HDX analysis monitored by the ultrahigh resolution Fourier transform ion cyclotron resonance mass spectrometry (FT-ICR MS)[31], including: automation[26,30], faster chromatographic separation[32], more efficient protein digestion[33], and enhanced data analysis[30]. Extension of HDX to higher molecular weight target proteins requires rapid elution of more peptide segments and dramatically increases mass spectral complexity. We therefore set out to study nucleotide-induced GroEL conformational changes in solution by amide backbone hydrogen/deuterium exchange coupled with mass spectrometry (HDX-MS). To access the GroEL complex, our analysis has been significantly enhanced through the use of ultra-high-resolution (and thus high peak capacity) 14.5 T FT-ICR MS[34].

Here, we complex ligand-free GroEL with ATPγS, a non-hydrolyzable ATP analog[35–37], to capture and mimic GroEL in its ATP-bound state. HDX data from the ligand-bound state and apo GroEL may then be interpreted based on available X-ray crystallographic structures to provide comprehensive characterization of nucleotide-induced solution-phase GroEL conformational changes.

Results

HDX-MS analysis of nucleotide-regulated GroEL. By use of a combination of protease XIII and urea denaturant optimized to yield maximum proteolytic sequence coverage[38], we identified more than 500 peptides for both apo GroEL and ATPγS-bound GroEL. Altogether, 134 peptides common to both apo- and liganded proteins and containing fewer than 30 amino acid residues were chosen for data analysis (Supplementary Fig. 1 and Supplementary Table 1). Averaged relative difference in deuterium uptake (ARDD) was calculated (Fig. 1) for each peptide from apo and liganded GroEL as described previously[39]. ARDD values for each GroEL peptide are color-coded and mapped onto the GroEL sequence in Fig. 1. The 134 overlapping peptides provide ~99% sequence coverage, including the C-terminus unstructured region 527–548, thus providing access to structural changes throughout the protein assembly.

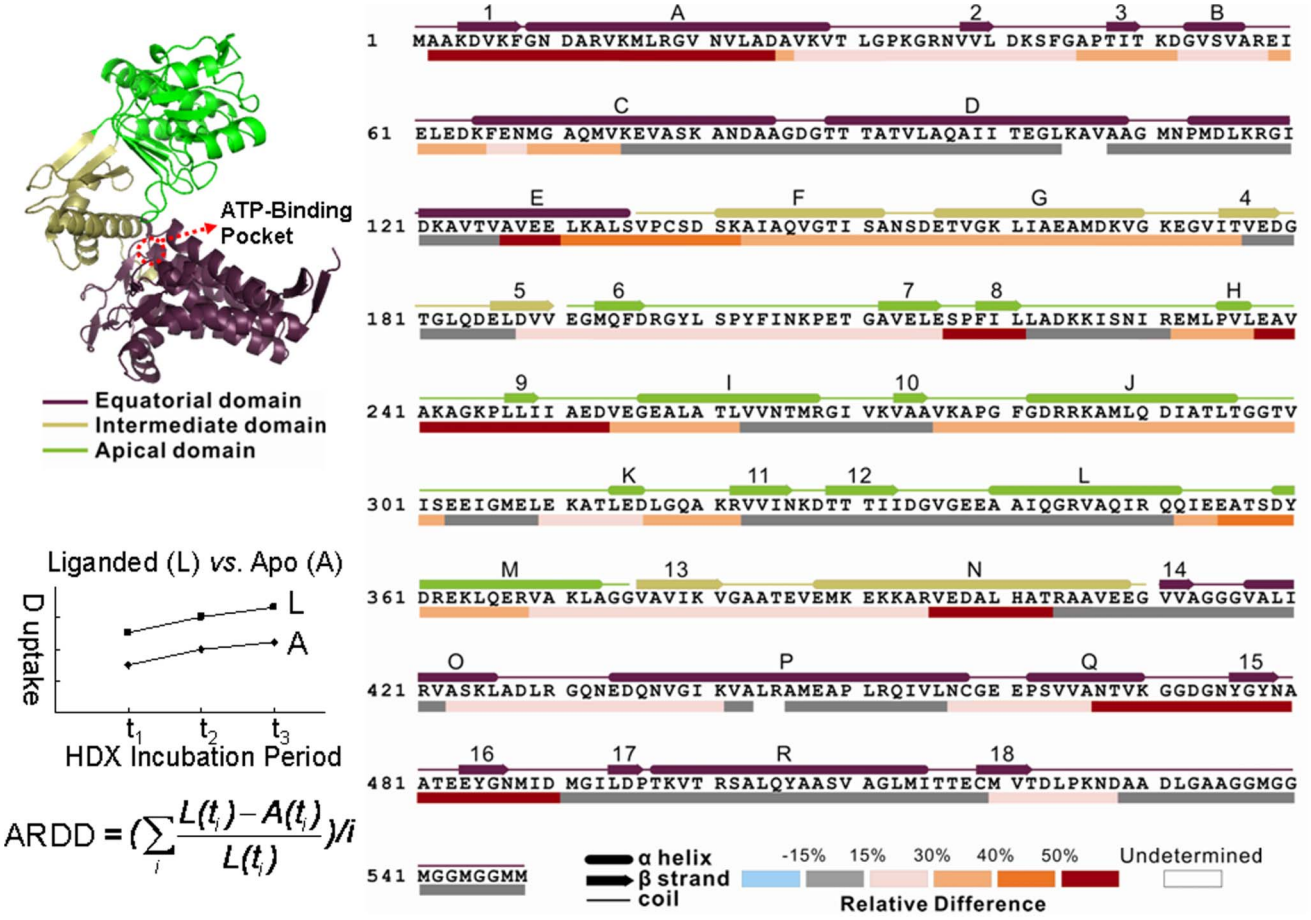

Figure 1 | H/D exchange results for three GroEL domains. The structural elements are identified above the sequence with 3 domains colored as in the top left GroEL monomer x-ray crystal structure, with line format designating helix/beta strand/random coil. For each of the proteolytic peptides common to apo GroEL and GroEL-ATPγS, the relative D-uptake difference (ARDD, liganded minus apo, averaged over all HDX incubation periods, t_i) is calculated as shown in the bottom left equation. The results from all peptides are combined such that short peptides are mapped below the sequence and longer peptides are then chosen to fill any gaps. Color coding for ARDD values is shown at bottom right.

Structural asymmetry of the nucleotide-bound GroEL. Deuterium uptake for a given peptide after a particular HDX period is calculated as the increase in the abundance weighted average mass of its isotopic distribution relative to that for the unlabeled peptide (the blank control). Interestingly, some of the peptide isotopic distributions are bimodal for GroEL-ATPγS, but not for apo GroEL (e.g., Fig. 2, peptide 6–13). Notably, the bimodal pattern applies only to those regions that exhibit conformational change upon ligand binding (Fig. 2, peptide 117–127). Furthermore, for those GroEL-ATPγS peptides showing a bimodal distribution, the lower mass segment of the distribution is similar to the isotopic envelope for apo GroEL (Fig. 2, peptide 387–406).

A bimodal distribution could result from EX1 type HDX kinetics[25,28], in which two distinct protein conformations interconvert during the HDX incubation period. In our case the GroEL conformation is fixed by incubating the ligand with GroEL for 30 min prior to HDX, whereas ATP-induced conformational changes are reported to have a rate constant of $\sim 10\ s^{-1}$ [40], which is too fast to be captured by the present HDX MS technique. Rather, the observed bimodal distribution may be ascribed to structural differences between the two heptameric rings caused by ATP binding to one ring. Previous studies indicate that nucleotide may bind to only one GroEL ring[6,7,41–43] despite an earlier X-ray structure indicating one ATPγS per GroEL monomer[19]. Such structural asymmetry of nucleotide-bound GroEL persists for HDX experiments at higher nucleotide concentration. As shown in Supplementary Fig. 2, when the protein 14-mer is saturated by 14 ATPγS, the two GroEL rings maintain different conformations. Consistent with that HDX result, the cryo-EM captured ATP-bound GroEL also indicates that one ATP bound GroEL ring is in a relaxed state whereas the other ring is in a tense state[44]. In the EM structure, the tense state ring is structurally more similar to a ring of apo GroEL, whereas several inter-subunit contacts are found to be lost in the relaxed state ring. Taking into account all of the discussed evidence, we interpret that the bimodal distribution is the result of structural asymmetry between the two GroEL rings.

Specific changes in GroEL structure induced by nucleotide binding. The sensitivity of the present approach to structural differences depends on both the solvent exposure for a specific residue and the secondary structure. For example, moving a loop from a buried position to a more open location will be detected by HDX-MS. Here, we simply report conformational changes, whether they originate from a change in secondary structure or solvent exposure. Based on the extent of deuterium uptake difference, specific GroEL regions can be categorized as having "major" (>50%) or "minor" (15%–50%) nucleotide-induced conformational changes. Such changes are observable in all three functional domains of GroEL, indicating that the changes induced by nucleotides binding are global. In Fig. 3, the various regions are mapped onto a three dimensional x-ray crystal structure of GroEL[1].

In the equatorial domain, there are 2 major and 3 minor changed regions upon nucleotide binding. The most dramatic change occurs in helix A and β strand 1 (Fig. 3, I), revealed by a group of overlapping peptides spanning residues 2 to 29. In particular, peptides 6–13 (also shown in Fig. 2), 16–23, and 18–25 display deuterium uptake differences greater than 60%. Interestingly, residues Val 6 and Val 22 constitute a pair of inter-subunit contacts in the same ring[1] and the mutation on Ala 3 has been shown to cause a functional defect, possibly by disrupting communication between neighboring subunits[45]. The second major changed region is 459–487 (Fig. 3, II), from part of helix Q and β strand 15/16. The representative peptides are 459–466 (Fig. 2) and 467–490, in which the residues Glu 461, Ser 463, and Val 464 are involved in the inter-ring interaction between two subunits[1]. The 3 minor changed regions are 38–65 (β strand 2/3 and

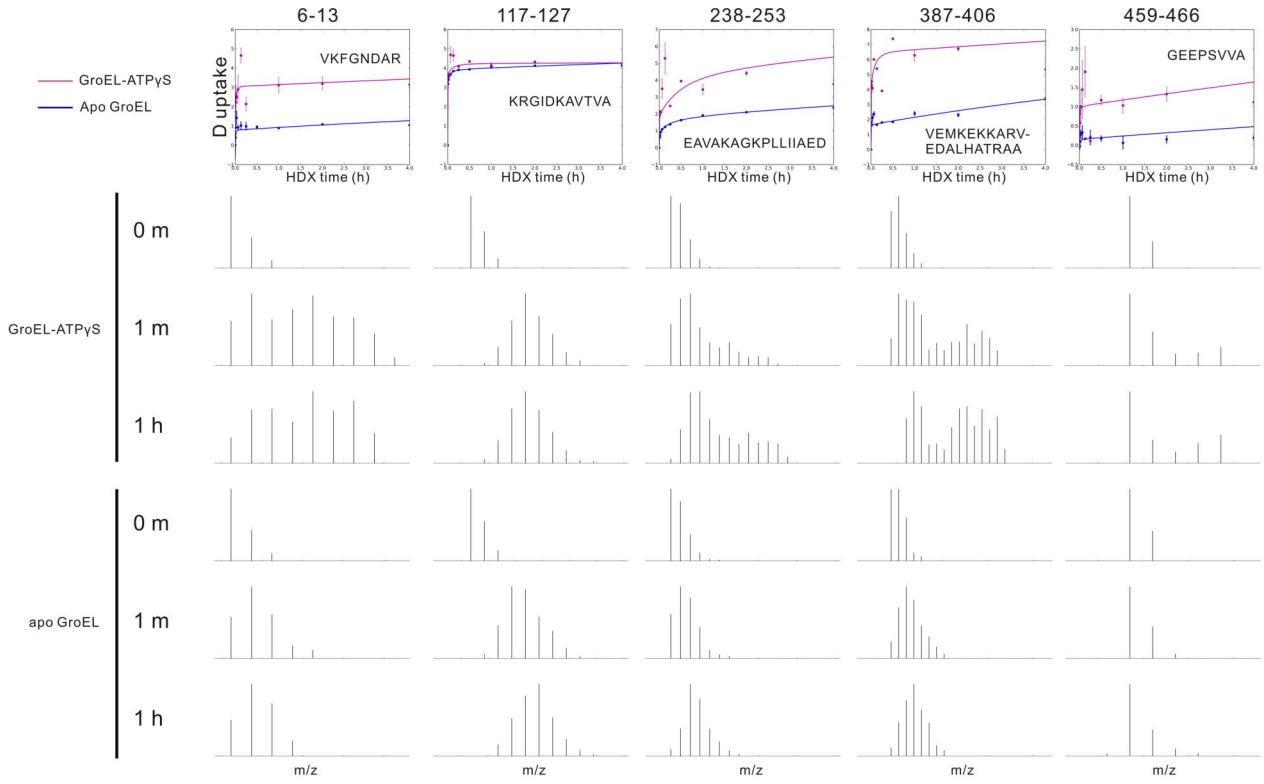

Figure 2 | Deuterium incorporation vs. H/D exchange period for five representative peptides, along with HDX mass spectra for at three indicated incubation periods. For each peptide exhibiting significant difference in HDX behavior between apo GroEL and GroEL-ATPγS (e.g., peptides 6-13, 238-253, 387-406, and 459-466), a clear bimodal isotopic distribution is observed. However, for peptide 117-127 which is unaffected by nucleotide binding, a single isotopic distribution is observed.

Regions	I	II	III	IV	V
Representative Peptides	6-13 16-23	459-466	46-52	422-441 425-440	515-530 522-528

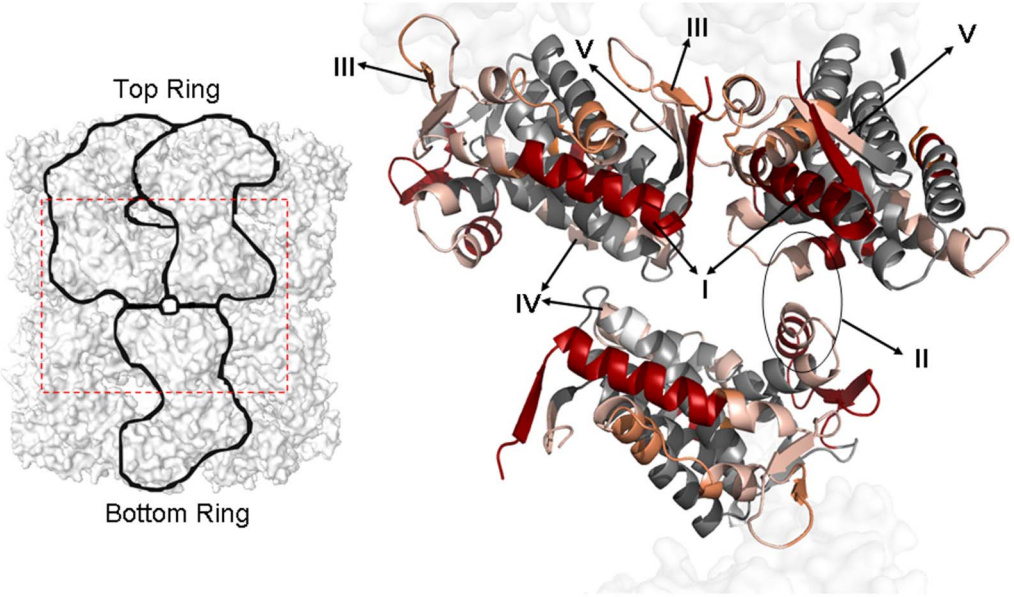

Figure 3 | The equatorial domains in three interacting GroEL subunits. Five regions (I-V) from the HDX comparison of GroEL-ATPγS vs. apo GroEL are colored as in Fig. 1. Two subunits in the top GroEL ring and one in the bottom ring are chosen to represent the inter-subunit and inter-ring interactions (viewed from the outside of the cylinder). Representative peptides for the regions are shown in the inset table.

helix B, Fig. 3, III), 422–441 (part of helix O/P and their linker, Fig. 3, IV), and 520–528 (β strand 18 Fig. 3, V), all exhibiting significant increase in deuterium uptake by GroEL-ATPγS. The β2/β3 stem loop is slightly shifted in the crystal structure of GroEL-ATPγS[19] compared with the crystal structure of apo GroEL[1]. Residues 36–40 from β strand 2/3 are also in contact with residues 516 and 518–522 near β strand 18 in a neighboring subunit[1], and collectively form a β sheet, as shown in Fig. 3, III and V. The first residue in helix P (shown in Fig. 3, IV), Glu 434, participates in the inter-ring interaction[1].

In the intermediate domain, β strand 4, 5, and 13 exhibit minor changes and part of helix N (Fig. 2 peptide 387–406) shows major changes. The small intermediate domain connects the apical domain and equatorial domain and forms part of the outer circumference of the cylinder. The short antiparallel β strands 4, 5, and 13 (Fig. 4, I) function as the covalent linker between the two domains. The minor D-uptake change observed for β strands 4, 5, and 13 may indicate that they function as a communicator between the apical and equatorial domains during the allosteric regulation. The changed β strands are likely the key regions that facilitate the 10° rotation of the intermediate domain observed in the cryo-EM captured ATP-bound state[44]. The helix N (Fig. 4, II) is in contact with the apical domain of the neighboring subunit, and the major change in deuterium uptake may indicate an altered inter-subunit interaction.

For the apical domain, several changed regions are observed. The changed regions are 190–221 (β strands 6, 7, and 8 with linker, Fig. 4, III), 238–252 (β strand 9 with flanking loop, Fig. 4, IV), 275–302 (β strand 10 and helix J, Fig. 4, V), and 352–367 (part of helix M, Fig. 4, VI). Several residues from regions 190–221, 275–302, and 352–367 (Phe 281, Try 360, Arg 197, and Arg 285) are in contact with helix N of the intermediate domain from the neighboring subunit in the 3D model, indicating that the interaction might be weakened upon nucleotide binding. From the crystallographic model, the portions of the apical domain facing the channel and the top surface of the cylinder may be inherently flexible, enabling them to accommodate a variety of unfolded peptide substrates[1]. The residues 238–252 (Fig. 2, peptide 238–253) near β strand 9 (Fig. 4, IV) lie on the edge of the channel entrance, and their flexibility and/or solvent accessibility is further enhanced upon nucleotide binding. This structural change may indicate conformational rearrangement enabling GroES to bind a substrate protein. The conformational change for region 238–252 explains the radial expansion of the channel entrance in the allosteric R ring observed by cryo-EM[44].

Discussion

The HDX-MS data herein reveal a much more detailed picture of nucleotide regulated wild type GroEL structure than any previous effort. Allosteric conformational changes are resolved to as few as several amino acid positions in solution, whereas previous cryo-EM studies have observed structural changes only at the domain or subdomain level. Moreover, the HDX-MS experiments have been optimized to achieve ~99% sequence coverage and to reveal detailed structural differences between the two GroEL conformational states. The overall solvent accessibility and/or structure flexibility of GroEL-ATPγS is enhanced relative to apo GroEL, as indicated by higher deuterium uptake levels throughout the sequence upon nucleotide binding. Multiple regions with different structural function are identified as changed in ATPγS-bound GroEL.

A major effect of nucleotide binding is significant weakening of the interaction between the GroEL subunits within one ring. The weakened intra-ring interaction was also observed by cryo-EM, in which the intermediate domain of one ring rotates significantly and its inter-subunit contact between intermediate and apical domains is lost[44]. Another major effect is that the interaction between the two GroEL rings is weakened. Notably, prior cryo-EM study also revealed that the two rings move apart upon ATP binding, but the present HDX-MS results pinpoint the detailed sequence composition responsible for such domain movement (Fig. 3, II).

Regions	I	II	III	IV	V	VI
Representative Peptides	173-180 369-380	387-406	193-221	238-253	277-293	355-368

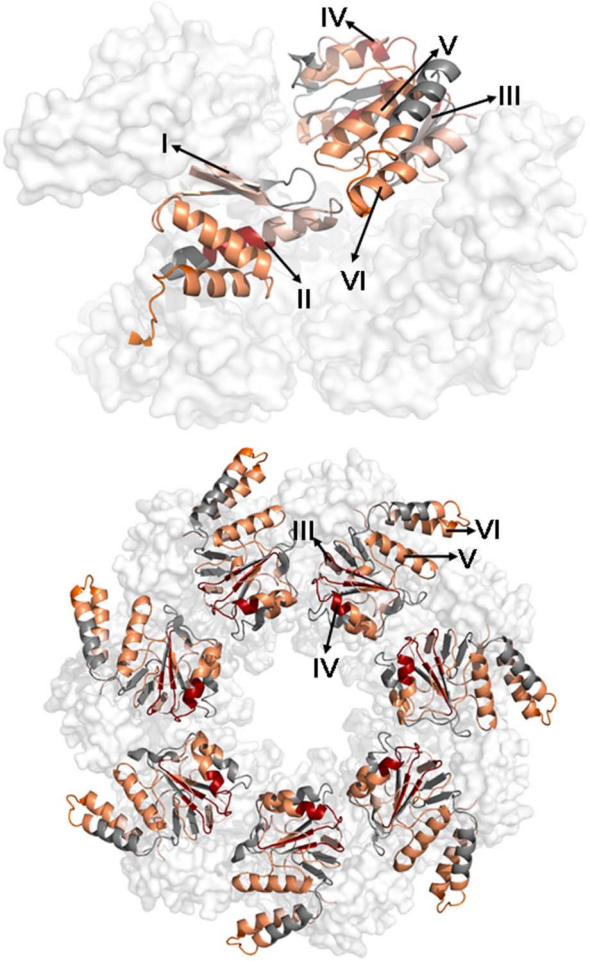

Figure 4 | Top: Apical domain (right monomer) and intermediate domain (left monomer). Bottom: Top view of one GroEL ring colored for the apical domain. The representative peptides for the regions are shown in the inset table. Color coding is as in Fig. 1.

Relatively minor conformational changes are seen for the short antiparallel β strands in the intermediate domain and the portion of the apical domain forming the channel entrance. Conformational change in the intermediate domain β strands may explain the domain rotation previously observed by cryo-EM. Interestingly, the channel entrance is observed to be more flexible upon nucleotide binding, to facilitate subsequent entry of a substrate protein.

Methods

GroEL and nucleotides. Wild-type GroEL was expressed in *E. coli* BL21 (DE3) cells. The protein was purified to homogeneity as reported previously[6,41,46]. Protein quality was verified by SDS polyacrylamide gel electrophoresis with both Coomassie-brilliant blue and silver staining. The commercial nucleotide, ATPγS (Sigma), was further purified to remove commercial contaminants by HPLC. Briefly, a nucleotide stock in 50 mM ammonium carbonate was applied to a self-packed Q-sepharose anion-exchange column (GE. Healthcare Bio-Sciences AB, Uppsala, Sweden) and eluted with a linear gradient of 50–500 mM ammonium carbonate. The nucleotide-containing fractions were pooled and lyophilized.

Hydrogen/deuterium exchange. A stock solution of ~10 μM GroEL tetradecamer was prepared in a standard buffer containing 20 μM HEPES, pH 7.5 in H_2O. Apo-GroEL and GroEL-ATPγS were prepared at equal protein concentration at final salt concentrations of 10 mM KCl and 10 mM $MgCl_2$, with or without 500 μM ATPγS, and incubated on ice for 30 min. Similar buffer conditions were applied for the preparation of the corresponding D_2O buffers, except that the nucleotide concentration was reduced to 50 μM.

The HDX experiments for apo GroEL and GroEL-ATPγS were optimized and automated with an HTC Pal autosampler (Eksigent Technologies, Dublin, CA). 5 μL of GroEL or GroEL-ATPγS was mixed with 45 μL of corresponding buffer in D_2O to initiate each H/D exchange period. For the blank control, the initial dilution was made in H_2O buffer. The HDX incubation periods were 0.5, 1, 2, 4, 8, 15, 30, 60, 120, 240, and 480 min, each followed by simultaneous quench and proteolysis. Each 50 μL sample was quenched by rapid mixing with 25 μL of 200 mM TCEP, 8 M urea in 1.0% formic acid, and 25 μL of a five-fold dilution of saturated protease type XIII in 1.0% formic acid (final pH ~2.3) Protease digestion was performed for 2 min followed by injection for LC-MS analysis. Each HDX reaction and assay was performed in triplicate. All HDX experiments were performed at ~1°C controlled by a Huber power water bath (Peter Huber, Offenburg, Germany).

On-line LC ESI FT-ICR MS. After proteolysis, the GroEL peptides were separated and desalted with a Jasco HPLC/SFC instrument (Jasco, Easton, MD) interfaced with an HTC Pal autosampler (Eksigent Technologies, Dublin, CA)[30]. For LC, 45 μL of the protein digest was injected from a 50 μL loop to a Pro-Zap Expedite MS C_{18} column (Grace Davidson, Deerfield, IL), HR 1.5 μm particle size, 500 Å, and pore size, 2.1 × 10 mm. A rapid gradient from 2% B to 95% B in 1.5 min (A: acetonitrile/H_2O/formic acid, 5/94.5/0.5 v/v; B: acetonitrile/H_2O/formic acid, 95/4.5/0.5 v/v) was performed at a flow rate of 0.3 mL/min. The LC eluent flow rate was reduced by ~1/1000 by a post-column splitter for efficient microelectrospray ionization (micro-ESI)[47].

The ionized LC eluent was directed to a custom-built hybrid LTQ 14.5 T FT-ICR mass spectrometer (ThermoFisher, San Jose, CA)[34]. Mass spectra were collected from m/z 380 – 1300 at high mass resolving power ($m/\Delta m_{50\%}$ = 100,000 at m/z 400, in which $\Delta m_{50\%}$ is mass spectral peak full width at half-maximum peak height). The total data acquisition period for each sample was 6.5 min (319 acquisitions). External ion accumulation[48] was performed in the linear ion trap with a target ion population

of three million charges for each FT-ICR measurement. LTQ-accumulated ions were transferred (~1 ms transfer period)[49] through three octopole ion guides (2.2 MHz, 250 V_{p-p}) to a capacitively coupled[50] open cylindrical ICR cell (55 mm i.d.) for mass spectral analysis. The ion accumulation period was typically less than 100 ms during peptide elution and the FT-ICR time-domain signal acquisition period was 767 ms (i.e., an overall duty cycle of ~1 Hz per acquisition). Automatic gain control[51] and high magnetic field[52] provided excellent external calibration[53] mass accuracy (normally better than 500 ppb rms mass error).

HDX data analysis. Data were acquired with Xcalibur software (Thermo-Fisher) and analyzed by a custom algorithm[30]. For each deuterium-labeled peptide, each isotopic distribution was visualized by a Python script to determine deuterium uptake. Time-course deuterium incorporation profiles were fitted by a maximum entropy method[54].

1. Braig, K. *et al*. The crystal structure of the bacterial chaperonin GroEL at 2.8 A. *Nature* **371**, 578–586 (1994).
2. Hartl, F. U., Bracher, A. & Hayer-Hartl, M. Molecular chaperones in protein folding and proteostasis. *Nature* **475**, 324–332 (2011).
3. Horwich, A. L., Farr, G. W. & Fenton, W. A. GroEL-GroES-mediated protein folding. *Chem. Rev.* **106**, 1917–1930 (2006).
4. Walter, S. & Buchner, J. Molecular chaperones - Cellular machines for protein folding. *Angew. Chem. Int. Ed.* **41**, 1098–1113 (2002).
5. Richter, K., Haslbeck, M. & Buchner, J. The heat shock response: life on the verge of death. *Mol. Cell* **40**, 253–266 (2010).
6. Chen, J., Makabe, K., Nakamura, T., Inobe, T. & Kuwajima, K. Dissecting a bimolecular process of MgATP(2-) binding to the chaperonin GroEL. *J. Mol. Biol.* **410**, 343–356 (2011).
7. Clare, D. K. *et al*. ATP-Triggered conformational changes delineate substrate-binding and -folding mechanics of the GroEL chaperonin. *Cell* **149**, 113–123 (2012).
8. Grason, J. P., Gresham, J. S., Widjaja, L., Wehri, S. C. & Lorimer, G. H. Setting the chaperonin timer: The effects of K^+ and substrate protein on ATP hydrolysis. *Proc. Nat. Acad. Sci. U.S.A.* **105**, 17334–17338 (2008).
9. Kim, S. Y., Miller, E. J., Frydman, J. & Moerner, W. E. Action of the chaperonin GroEL/ES on a non-native substrate observed with single-molecule FRET. *J. Mol. Biol.* **401**, 553–563 (2010).
10. Rostom, A. A. & Robinson, C. V. Detection of the intact GroEL chaperonin assembly by mass spectrometry. *J. Am. Chem. Soc.* **121**, 4718–4719 (1999).
11. Tyagi, N. K., Fenton, W. A. & Horwich, A. L. GroEL/GroES cycling: ATP binds to an open ring before substrate protein favoring protein binding and production of the native state. *Proc. Nat. Acad. Sci. U.S.A.* **106**, 20264–20269 (2009).
12. Shtilerman, M., Lorimer, G. H. & Englander, S. W. Chaperonin function: folding by forced unfolding. *Science* **284**, 822–825 (1999).
13. Illingworth, M., Ramsey, A., Zheng, Z. & Chen, L. Stimulating the substrate folding activity of a single ring GroEL variant by modulating the cochaperonin GroES. *J. Biol. Chem.* **286**, 30401–30408 (2011).
14. Fiaux, J., Bertelsen, E. B., Horwich, A. L. & Wuthrich, K. NMR analysis of a 900K GroEL-GroES complex. *Nature* **418**, 207–211 (2002).
15. Horovitz, A. & Willison, K. R. Allosteric regulation of chaperonins. *Curr. Opin. Struct. Biol.* **15**, 646–651 (2005).
16. Hyeon, C., Lorimer, G. H. & Thirumalai, D. Dynamics of allosteric transitions in GroEL. *Proc. Nat. Acad. Sci. U.S.A.* **103**, 18939–18944 (2006).
17. Ranson, N. A. *et al*. Allosteric signaling of ATP hydrolysis in GroEL-GroES complexes. *Nat. Struct. Mol. Biol.* **13**, 147–152 (2006).
18. Kim, S. Y. *et al*. Probing the sequence of conformationally induced polarity changes in the molecular chaperonin GroEL with fluorescence spectroscopy. *J. Phys. Chem. B* **109**, 24517–24525 (2005).
19. Boisvert, D. C., Wang, J., Otwinowski, Z., Horwich, A. L. & Sigler, P. B. The 2.4 A crystal structure of the bacterial chaperonin GroEL complexed with ATP gamma S. *Nat. Struct. Biol.* **3**, 170–177 (1996).
20. Wang, J. & Boisvert, D. C. Structural basis for GroEL-assisted protein folding from the crystal structure of (GroEL-KMgATP)(14) at 2.0 angstrom resolution. *J. Mol. Biol.* **327**, 843–855 (2003).
21. Inobe, T., Kikushima, K., Makio, T., Arai, M. & Kuwajima, K. The allosteric transition of GroEL induced by metal fluoride-ADP complexes. *J. Mol. Biol.* **329**, 121–134 (2003).
22. Engen, J. R. & Smith, D. L. Investigating protein structure and dynamics by hydrogen exchange MS. *Anal. Chem.* **73**, 256A–265A (2001).
23. Frantom, P. A., Zhang, H. M., Emmett, M. R., Marshall, A. G. & Blanchard, J. S. Mapping of the allosteric network in the regulation of alpha-isopropylmalate synthase from Mycobacterium tuberculosis by the feedback inhibitor L-leucine: solution-phase H/D exchange monitored by FT-ICR mass spectrometry. *Biochemistry* **48**, 7457–7464 (2009).
24. Houde, D., Arndt, J., Domeier, W., Berkowitz, S. & Engen, J. R. Characterization of IgG1 conformation and conformational dynamics by hydrogen/deuterium exchange mass spectrometry. *Anal. Chem.* **81**, 5966 (2009).
25. Zhang, Z. & Smith, D. L. Determination of amide hydrogen exchange by mass spectrometry: a new tool for protein structure elucidation. *Protein Sci.* **2**, 522–531 (1993).
26. Chalmers, M. J. *et al*. Probing protein ligand interactions by automated hydrogen/deuterium exchange mass spectrometry. *Anal. Chem.* **78**, 1005–1014 (2006).
27. Lanman, J. *et al*. Identification of novel interactions in HIV-1 capsid protein assembly by high-resolution mass spectrometry. *J. Mol. Biol.* **325**, 759–772 (2003).
28. Lanman, J. *et al*. Key interactions in HIV-1 maturation identified by hydrogen-deuterium exchange. *Nat. Struct. Mol. Biol.* **11**, 676–677 (2004).
29. Lisal, J. *et al*. Interaction of packaging motor with the polymerase complex of dsRNA bacteriophage. *Virology* **351**, 73–79 (2006).
30. Kazazic, S. *et al*. Automated data reduction for hydrogen/deuterium exchange experiments, enabled by high-resolution Fourier transform ion cyclotron resonance mass spectrometry. *J. Am. Soc. Mass. Spectrom.* **21**, 550–558 (2010).
31. Marshall, A. G., Hendrickson, C. L. & Jackson, G. S. Fourier transform ion cyclotron resonance mass spectrometry: a primer. *Mass Spectrom. Rev.* **17**, 1–35 (1998).
32. Zhang, H. M., Bou-Assaf, G. M., Emmett, M. R. & Marshall, A. G. Fast reversed-phase liquid chromatography to reduce back exchange and increase throughput in H/D exchange monitored by FT-ICR mass spectrometry. *J. Am. Soc. Mass Spectrom.* **20**, 520–524 (2009).
33. Zhang, H. M. *et al*. Enhanced digestion efficiency, peptide ionization efficiency, and sequence resolution for protein hydrogen/deuterium exchange monitored by Fourier transform ion cyclotron resonance mass spectrometry. *Anal. Chem.* **80**, 9034–9041 (2008).
34. Schaub, T. M. *et al*. High-performance mass spectrometry: Fourier transform ion cyclotron resonance at 14.5 Tesla. *Anal. Chem.* **80**, 3985–3990 (2008).
35. Yifrach, O. & Horovitz, A. Transient kinetic analysis of adenosine 5'-triphosphate binding-induced conformational changes in the allosteric chaperonin GroEL. *Biochemistry* **37**, 7083–7088 (1998).
36. Meyer, A. S. *et al*. Closing the folding chamber of the eukaryotic chaperonin requires the transition state of ATP hydrolysis. *Cell* **113**, 369–381 (2003).
37. Hessling, M., Richter, K. & Buchner, J. Dissection of the ATP-induced conformational cycle of the molecular chaperone Hsp90. *Nat. Struct. Mol. Biol.* **16**, 287–293 (2009).
38. Zhang, H. M. *et al*. Drug binding and resistance mechanism of KIT tyrosine kinase revealed by hydrogen/deuterium exchange FT-ICR mass spectrometry. *Protein Sci.* **19**, 703–715 (2010).
39. Zhang, Q. *et al*. Epitope mapping of a 95 kDa antigen in complex with antibody by solution-phase amide backbone hydrogen/deuterium exchange monitored by Fourier transform ion cyclotron resonance mass spectrometry. *Anal. Chem.* **83**, 7129–7136 (2011).
40. Inobe, T. *et al*. Equilibrium and kinetics of the allosteric transition of GroEL studied by solution X-ray scattering and fluorescence spectroscopy. *J. Mol. Biol.* **327**, 183–191 (2003).
41. Inobe, T., Makio, T., Takasu-Ishikawa, E., Terada, T. P. & Kuwajima, K. Nucleotide binding to the chaperonin GroEL: non-cooperative binding of ATP analogs and ADP, and cooperative effect of ATP. *Biochim. Biophys. Acta, Protein Struct. Mol. Enzymol.* **1545**, 160–173 (2001).
42. Chaudhry, C. *et al*. Role of the gamma-phosphate of ATP in triggering protein folding by GroEL-GroES: function, structure and energetics. *EMBO J.* **22**, 4877–4887 (2003).
43. Cliff, M. J. *et al*. A kinetic analysis of the nucleotide-induced allosteric transitions of GroEL. *J. Mol. Biol.* **293**, 667–684 (1999).
44. Ranson, N. A. *et al*. ATP-bound states of GroEL captured by cryo-electron microscopy. *Cell* **107**, 869–879 (2001).
45. Horovitz, A., Bochkareva, E. S., Kovalenko, O. & Girshovich, A. S. Mutation Ala2-->Ser destabilizes intersubunit interactions in the molecular chaperone GroEL. *J. Mol. Biol.* **231**, 58–64 (1993).
46. Chen, J. *et al*. Fibrillogenic propensity of the GroEL apical domain: a Janus-faced minichaperone. *FEBS Lett.* **586**, 1120–1127 (2012).
47. Emmett, M. R. & Caprioli, R. M. Microelectrospray mass spectrometry: ultra-high-sensitivity analysis of peptides and proteins. *J. Am. Soc. Mass Spectrom.* **5**, 605–613 (1994).
48. Senko, M. W., Hendrickson, C. L., Emmett, M. R., Shi, S. D. H. & Marshall, A. G. External accumulation of ions for enhanced electrospray ionization Fourier transform ion cyclotron resonance mass spectrometry. *J. Am. Soc. Mass Spectrom.* **8**, 970–976 (1997).
49. Wilcox, B. E., Hendrickson, C. L. & Marshall, A. G. Improved ion extraction from a linear octopole ion trap: SIMION analysis and experimental demonstration. *J. Am. Soc. Mass Spectrom.* **13**, 1304–1312 (2002).
50. Beu, S. C. & Laude, D. A. Elimination of axial ejection during excitation with a capacitively coupled open trapped-ion cell for Fourier transform ion cyclotron resonance mass spectrometry. *Anal. Chem.* **64**, 177–180 (1992).
51. Schwartz, J. C., Senko, M. W. & Syka, J. E. A two-dimensional quadrupole ion trap mass spectrometer. *J. Am. Soc. Mass Spectrom.* **13**, 659–669 (2002).
52. Marshall, A. G. & Guan, S. Advantages of high magnetic field for Fourier transform ion cyclotron resonance mass spectrometry. *Rapid Commun. Mass Spectrom.* **10**, 1819–1823 (1996).
53. Ledford, E. B., Jr., Rempel, D. L. & Gross, M. L. Space charge effects in Fourier transform mass spectrometry. Mass calibration. *Anal. Chem.* **56**, 2744–2748 (1984).
54. Zhang, Z., Li, W., Logan, T. M., Li, M. & Marshall, A. G. Human recombinant [C22A] FK506-binding protein amide hydrogen exchange rates from mass

spectrometry match and extend those from NMR. *Protein Sci.* **6**, 2203–2217 (1997).

Acknowledgments

This work was supported by NSF Division of Materials Research through DMR-06-54118 and the State of Florida, and also in part by a Grant-in-Aid for Scientific Research in Innovative Areas (project number: 20107009) from the Ministry of Education, Culture, Sports, Science and Technology of Japan.

Author contributions

J.C. prepared the apo- and complexed GroEL protein. J.C. prepared GroEL and purified nucleotide samples. Q.Z. and H.-M.Z. designed the HDX experiments and Q.Z. performed the experiments. Q.Z., J.C. and H.-M.Z. wrote the manuscript. F.X. performed phase correction to yield absorption-mode FT-ICR mass spectra. A.G..M., N.L.Y. and K.K. oversaw all research phases and revised the manuscript. All authors discussed and improved the manuscript.

Additional information

Supplementary information accompanies this paper at http://www.nature.com/scientificreports

Competing financial interests: The authors declare no competing financial interests.

License: This work is licensed under a Creative Commons Attribution-NonCommercial-NoDerivs 3.0 Unported License. To view a copy of this license, visit http://creativecommons.org/licenses/by-nc-nd/3.0/

How to cite this article: Zhang, Q. *et al.* Nucleotide-induced conformational changes of tetradecameric GroEL mapped by H/D exchange monitored by FT-ICR mass spectrometry. *Sci. Rep.* **3**, 1247; DOI:10.1038/srep01247 (2013).